Research Article Vol. 32, No. 14 / 1 Jul 2024 / Optics Express 25091
Optics EXPRESS

Experimental evaluation of wearable LED strip and side-emitting fiber for optical camera communications systems

ELENI NIARCHOU,[1,†,*] KLARA EOLLOS-JAROSIKOVA,[2,†] VICENTE MATUS,[1] RAFAEL PEREZ-JIMENEZ,[1] STANISLAV ZVANOVEC,[2] MATEJ KOMANEC,[2] AND JOSE RABADAN[1]

[1]*Institute for Technological Development and Innovation in Communications, University of Las Palmas de Gran Canaria, Las Palmas de Gran Canaria 35001, Spain*
[2]*Department of Electromagnetic Field, Faculty of Electrical Engineering, Czech Technical University in Prague, Prague 16627, Czech Republic*
[†]These authors contributed equally to this work.
[*]*eleni.niarchou@ulpgc.es*

Abstract: This paper presents an experimental evaluation of two types of light-emitting diode (LED)-based distributed transmitters, namely an LED strip and an LED-coupled side-emitting optical fiber, in both laboratory and wearable optical camera communication (OCC) systems. We study the system performance in terms of success of reception (SoR) with regard to the transmission distance. The best value of SoR is achieved when the camera is facing directly to the transmitter (T_x) from a close distance of 1 m. Additionally, we compare the power consumption, the signal-to-noise ratio performance (SNR) and all the obtained values under optimal conditions are better than the forward error correction (FEC) limit in OCC systems.

1. Introduction

The widespread presence of smartphones equipped with cutting-edge cameras has prompted wider possibilities within optical wireless communications (OWC), particularly within the framework IEEE 802.15.7a [1]. This approach is known as optical camera communications (OCC) and employs a light-emitting diode (LED) as the transmitter (T_x), an image sensor (i.e., camera) as the receiver (R_x), and light as signal carrier.

OCC overcomes some of the limitations of Bluetooth and other existing radio frequency (RF)-based technologies [2], such as security and interference. A notable advantage lies in the fact that OCC does not incur additional hardware costs for the receiver as smartphones have been integrated with an embedded complementary metal oxide semiconductor (CMOS) camera in rolling shutter (RS) mode [3]. New generation smartphones can capture high-resolution photos and videos, with an average viewpoint resolution of 360×800 px [4], which means an actual resolution of 1080×2400 px and a recording speed of 30 frames per second (fps) or more, which is more than adequate for low-speed applications [5]. Moreover, the transmitter side can be implemented with a simple LED circuit, which has comparably lower complexity than the full Bluetooth circuitry.

Smart devices, including smartphones, smartwatches, and smart clothes, are viewed as products that integrate wearable technologies for recognizing human activities [6]. Wearable devices can be worn on the body, often designed to be lightweight and compact, offering convenience for users and seamless integration into clothing or accessories without disrupting their daily activities. These devices typically come equipped with sensors, processors, and communication capabilities, aiming to provide specific functionalities, such as tracking health and fitness metrics

#521967 https://doi.org/10.1364/OE.521967
Journal © 2024 Received 22 Feb 2024; revised 23 Apr 2024; accepted 11 May 2024; published 27 Jun 2024

Optics EXPRESS

[7]. Wearable health-monitoring sensors have become a part of our daily life [8,9] and represent a headstone for the Internet of Things (IoT) [10]. Sensors can measure parameters before the OCC system collects those data and forwards them to the camera from integrated light-emitting diodes. With the advent of 6G, the integration of wearables in healthcare is set to expand, paving the way for smart healthcare [11] in terms of sensing, processing, and communication.

To date, only a limited number of studies have explored the integration of wearable sensors in conjunction with LEDs as transmitters. For instance, in [12], medical sensors and infrared LEDs transmit medical data for patient monitoring. Similarly, in [13], this combination is used for indoor health monitoring, accounting for patient mobility. Additionally, in [14], an all-optical bidirectional wireless communication system assesses sensor mobility, variations in orientation, and placement on the body. Furthermore, in [15], the authors delve into the performance of optical code-division multiple access in asynchronous mode, considering the impact of mobility and random transmitter orientations. Moreover, in [16], optoelectric sensors monitor cardiovascular vital signs.

Recently, side-emitting optical fibers have been introduced as distributed transmitters for OCC [17,18]. Side-emitting fibers differ from conventional optical fibers by gradually emitting light along the side-emitting fiber length [19]. To achieve this glow-stick-like effect, the side-emitting fibers are modified by implementing scattering particles or voids into the side-emitting fiber core or cladding [20,21]. Side-emitting fibers are characterized by the so-called diffusion length, which is a side-emitting fiber length over which 90 % of the coupled power is emitted [22]. When using side-emitting fibers in OCC, a single LED is used to couple data into one end of the side-emitting fiber. The side-emitting fiber then acts as a distributed transmitter. Data is then captured by the RS camera, as in conventional OCC.

In the field of wearables, LED strips and LED-coupled side-emitting fibers represent two approaches to distributed transmitters. Both approaches have their advantages and drawbacks. Side-emitting optical fibers offer advantages such as 360° radiation pattern in contrast to 120° of LED strips. On the other hand, LED strips provide constant brightness in contrast to side-emitting fibers. LED strips are composed of multiple LEDs, offering flexibility in LED control, i.e., different spatial transmitting properties. Conversely, LED-coupled side-emitting fibers require only a single LED for their operation, allowing small and compact wearable solutions. Both types of distributed transmitters allow mechanical flexibility, while fiber-based transmitters in the future can be involved within textiles, multiple LEDs then could allow different shapes, etc. Apart from wearables, LED strips, and side-emitting fibers find applications in IoT, interior design [23], shopping centers, aircraft, fashion, health, safety, geolocation [24], promoting active lifestyles [25], and playing a role in industrial robotics [26]. In [27], the authors show the impact of a user moving with a camera receiver within cells at 20 cm/s speed.

In this work, we experimentally evaluate the above-mentioned types of LED-based distributed transmitters in laboratory and wearable OCC systems. We employ both solutions based on widely accessible and commercially available components, including LEDs, side-emitting fibers, and smartphones. The system performance of both wearable transmitters is evaluated and compared in terms of the success of reception, signal-to-noise ratio, and power consumption.

The structure of the paper is organized as follows. Section 2 provides details of the OCC system design and the experimental setup. Section 3 specifically focuses on the image processing techniques applied in the study. Section 4 is then dedicated to the discussion of the results obtained from the experiments with both transmitters. Lastly, Section 5 presents the main conclusions.

2. OCC system design and experimental setup

We consider two types of transmitters. The first transmitter is a 10 mm wide LED strip with a diffuser, consisting of an array of surface-mounted device white LEDs, 5.0 mm by 5.0 mm

Optics EXPRESS

size (commercially known as SMD 5050), operating at two different voltage states, 9 and 12 V (i.e., 432 mW and 720 mW electrical power, 50 mA and 60 mA current, respectively). This power supplies both the LED strip and the control circuit. The second transmitter is a side-emitting optical fiber. The side-emitting fiber ("Super Bright" by ZDEA) is made of polymethyl-methacrylate (PMMA) with a 3 mm outer diameter and with 1 m diffusion length, meaning that 90 % of the coupled power will be emitted from the fiber over the first 1 m side-emitting fiber length. An LED couples light to one end of the side-emitting fiber, and once the light is coupled, the side-emitting fiber becomes the data transmitter. The coupling LED operates at 3 V (i.e., 525 mW, 175 mA). Both T_xs are connected to the digital output of a micro-controller unit (MCU).

The proposed OCC system uses the non-return-to-zero on-off keying (NRZ-OOK) modulation technique [28] for data transmission over a free-space wireless channel of up to 2.5 m distance, which resembles a typical indoor scenario. However, the system can be extended even for longer distances (tens or hundreds of meters) [29]. We carry out experimental analysis both in ambient light and dark conditions. The system uses the digital switching outputs of the MCU to facilitate the NRZ-OOK modulation. The micro-controller generates a 6-bit data packet [001011] at 0.4 ms per bit, which corresponds to a modulation frequency of 2.5 kHz per bit. The data packet is converted into a voltage signal that directly drives the LED. Since the current of the LEDs in the LED strip, exceeds the maximum limit of the MCU, a transistor is connected to the power source to drive the LEDs. To enhance the link performance, a repeat-packet strategy is employed. For the LED strip experiments, the MCU is a Seeeduino Xiao [30], powered by the power supply unit, and for the LED-coupled side-emitting fiber experiments, the MCU is an Arduino Nano [31], powered by a laptop.

The receiver is a smartphone camera of Samsung A51 [32], which offers frame capture in pro mode, using 4000×1800 px resolution in rolling shutter mode. The OCC link scenario is depicted in Fig. 1. In OCC, the image is captured row-by-row using an RS camera. The RS camera exposes different lines of the image array at various times to read the light intensity through the sensor, enabling capturing multiple states of LEDs (ON and OFF) within a single frame [33]. The exposure time values of the camera (i.e., the duration of time over which a camera sensor line is exposed to light) are summarized in Table 1.

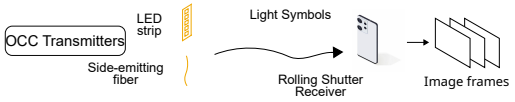

Fig. 1. Optical camera communications link scenario.

Table 1. Exposure times of the camera.

Experiment	Transmitter	Environment	t_{exp} (μs)
Laboratory	Strip (9 V)	ambient light	250
	Strip (12 V)	ambient light	250
	Side-emitting fiber	dark room	500
Wearable	Strip (9 V)	ambient light	170
	Strip (9 V)	dark room	170
	Strip (12 V)	ambient light	170
	Strip (12 V)	dark room	170
	Side-emitting fiber	ambient light	500
	Side-emitting fiber	dark room	500

Optics EXPRESS

The systems implemented for the proposed laboratory experiments are shown in Fig. 2, where both transmitters (1 m length) are placed horizontally. In the wearable experiments, a 50 cm length transmitter is vertically attached to the front side of a T-shirt, with direction from waist to shoulder, as shown in Fig. 3.

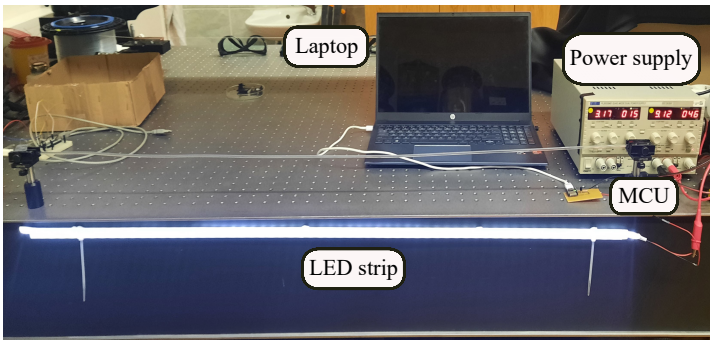

(a)

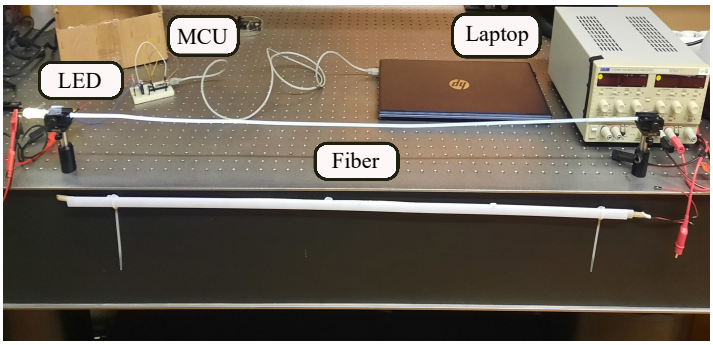

(b)

Fig. 2. Laboratory experimental setup. (a) LED strip. (b) LED-coupled side-emitting fiber.

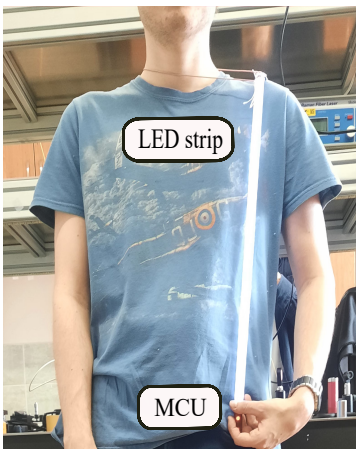

(a)

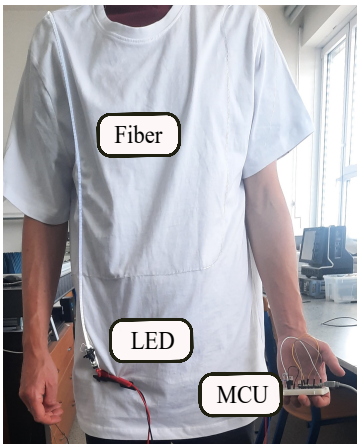

(b)

Fig. 3. Wearable experimental setup. (a) LED strip. (b) LED-coupled side-emitting fiber.

Optics EXPRESS

The measurements are illustrated in Fig. 4, with x and y representing the 2D coordinates of the room (in meters). The smartphone camera captures multiple frames of T_x from various distances, always focusing on the center of T_x at (0.0, 0.0). As the orientation of the T_xs is different in laboratory and wearable setups, each measurement tests different constraints by placing the camera accordingly. In the laboratory setup, we move the camera in the same plane where the T_x is placed, meaning we capture alongside the T_x. In wearable setup we move the camera in the plane that is perpendicular to the person wearing the T_x, meaning we capture images around the person. The most relevant parameters of the system are summarized in Table 2.

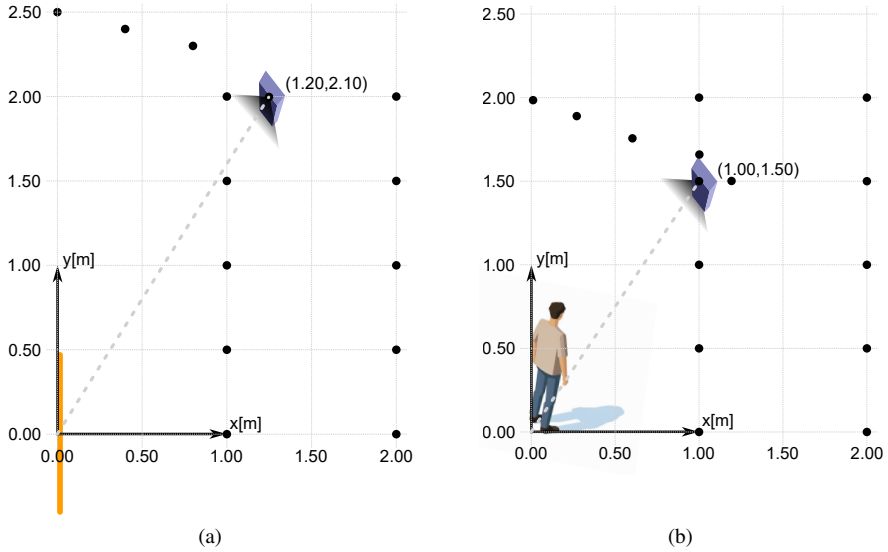

Fig. 4. The 2D coordinates of the room (in meters) represent the camera's capturing positions, always facing the center of the transmitter at (0.0, 0.0). (a) Laboratory experimental setup with a yellow line representing the T_x. (b) Wearable experimental setup with a person wearing the T_x on their T-shirt.

Table 2. Parameters of the system and their values.

Module	Sub-module	Parameter	Value
T_x	LED strip	LED	SMD 5050, white
		Width	10 mm
		Microcontroller	Seeeduino XIAO
	Side-emitting fiber	Diameter	4 mm
		LED	LA CW20WP6, white
		Material	PMMA
		Microcontroller	Arduino Nano
	Modulation	Modulation frequency	2.5 kHz
		Data packet size	6b/packet [001011]
R_x	Camera	Smartphone model	Samsung Galaxy A51
		Image sensor	Sony IMX582
		Resolution	4000×1800 px

Optics EXPRESS

3. Image processing

We used two different offline image processing techniques (see Fig. 5). Method 1 was developed especially for strip LED arrays. It uses for data recovery a template signal transmitted by the LED transmitter and detected within the image through a correlation process to find region of interest

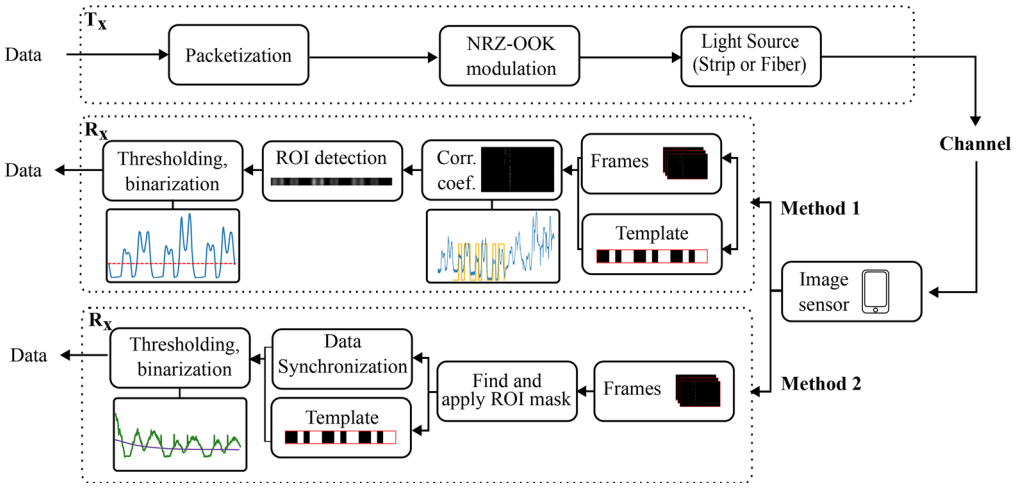

Fig. 5. Block diagram of the transmitting and receiving node.

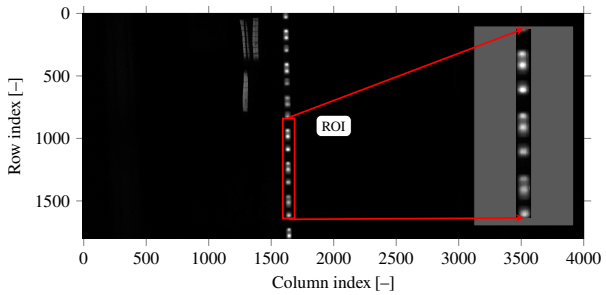

(a)

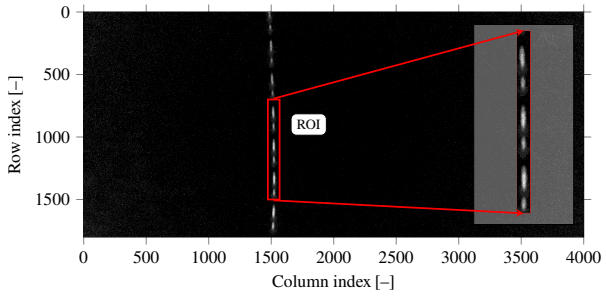

(b)

Fig. 6. Frame showing values obtained from the correlation coefficient between a random frame and the template. The region of interest (ROI) is highlighted. (a) LED strip. (b) LED-coupled side-emitting fiber. In both of the displayed images in this figure the contrast was increased to better show the transmitting data to the reader.

Optics EXPRESS

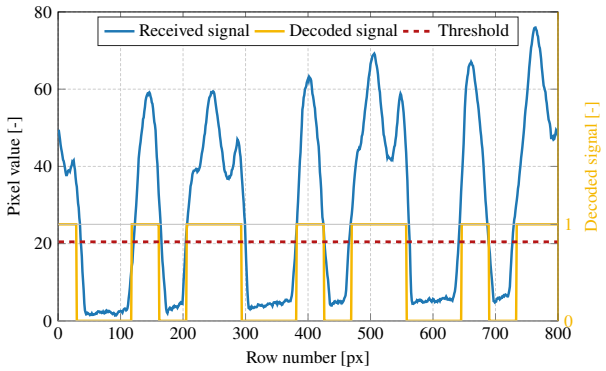

(a)

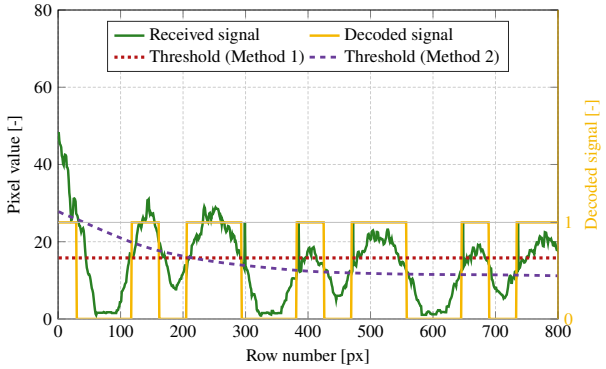

(b)

Fig. 7. Received grayscale signal, Decoded signal, and Thresholds for (a) LED strip and (b) side-emitting fiber (Method 1 and Method 2).

(ROI), while within Method 2, the ROI mask is determined by using the intensity information of the image.

In Method 1, one frame is selected while a template is generated, consisting of three consecutive packets, each with a sequence of [001011] bits. Image frames are then converted to grayscale, enabling retrieval of the pixels' intensity profile. The correlation process involves sliding the template image over the frame (similar to 2D convolution) to identify the 2D position of the signal captured from the transmitting source [34]. Figure 5 depicts a block diagram with T_x and R_x parts. The blue lines in inset within the R_x part of Fig. 5 represent the average row value, while the yellow line depicts the template signal, and the red line show binarization threshold. The ROI in the frame, where the correlation has the maximum value, is highlighted in Fig. 6. This process is repeated for all frames. The identified ROI is then utilized for data decoding. By applying thresholding and binarization to the acquired data, the received signal is efficiently decoded, as depicted in Fig. 7(a).

In Method 2, the mask is thereofore applied to the captured image using multiplication. From this image, a 1D data array with an intensity profile is generated. In this intensity profile, data synchronization is performed using the generated template. The synchronized data is binarized after thresholding. In Fig. 7(b), the binarization threshold is marked. Since the amount of light emitted from a side-emitting fiber decreases with increasing distance from the coupled light source (i.e., the LED) along the fiber, it is more suitable to use a moving average of intensity profile as the threshold instead of a constant threshold, which was used in Method 1. The

Optics EXPRESS

method for adapting the threshold value employed moving average based on the illumination level alongside the captured fiber. The same process is replicated for every frame. Efficient decoding of the received signal is achieved by employing the adaptive thresholding and binarization on the acquired data.

4. Results

In this section, we show the performance of both transmitters in terms of signal-to-noise ratio (SNR) and success of reception (SoR). Additionally, we measured the thermal radiation emanating from the transmitters using an infrared camera (by Teledyne FLIR).

The captured thermal images are depicted in Fig. 8 for the LED strip and in Fig. 9 for the side-emitting fiber. On both transmitters, the maximum thermal radiation is emitted at the starting point of the LED strip and at the LED holder for the side-emitting fiber, measuring 25.7° C and 31.3° C, respectively.

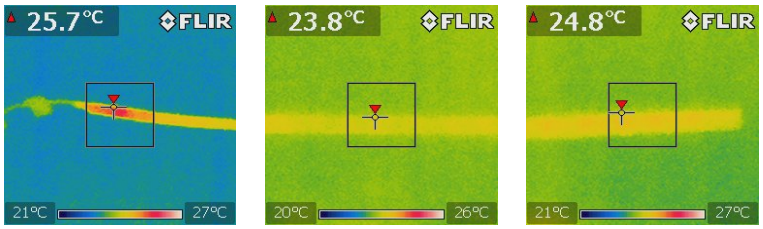

(a) (b) (c)

Fig. 8. Heat emanating from the entire length of the LED strip. (a) At the starting point. (b) In the middle section. (c) At the end.

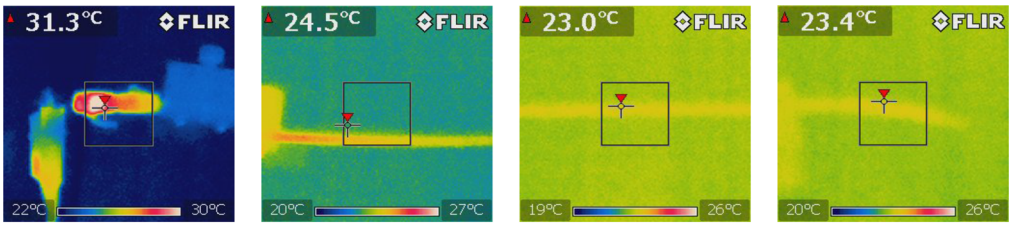

(a) (b) (c) (d)

Fig. 9. Heat emanating from the entire length of the side-emitting fiber. (a) At the LED holder. (b) At the starting point. (c) In the middle section. (d) At the end.

Based on measurements from the infrared camera, it can be inferred that there is no excessive overheating in any parts of both transmitters. The temperature of the transmitters was approximately at room temperature. However, the LED holder for side-emitting fiber could benefit from better heat-dissipation material.

To estimate the SNR, we captured frames using a direct connection of T_x to the power supply (i.e., the LEDs are driven only by a DC signal) at 2 m distance. Afterward, the frames were processed to align the T_x among the frames. Then, the image processing code calculated the average intensity of pixels for each row, representing the signal's mean value. The SNR was calculated as

$$\mathrm{SNR}_{\mathrm{dB}} = 10 \log_{10} \left(\frac{\mu^2}{\sigma^2} \right), \tag{1}$$

Optics EXPRESS

the ratio of the mean value of the signal μ, to the standard deviation σ, assuming that the aggregated noise distribution can be modeled as additive white Gaussian noise (AWGN). The SNR values for each experimental setup are summarized in Table 3.

Table 3. Signal to noise ratio (SNR) values.

Experiment	Transmitter	Environment	SNR [dB]
Laboratory	Strip (9 V)	ambient light	21.1
	Strip (12 V)	ambient light	22.0
	Fiber	ambient light	28.6 down to 13.3
Wearable	Strip (9 V)	ambient light	21.9
	Strip (9 V)	dark room	23.8
	Strip (12 V)	ambient light	21.9
	Strip (12 V)	dark room	27.4
	Fiber	ambient light	42.7 down to 19.3
	Fiber	dark room	42.9 down to 20.2

In the laboratory experiment, the SNR is almost the same for the LED strip at 9 and 12 V (21.1 and 22.0 dB, respectively), while the side-emitting fiber exhibited a range from 28.6 down to 13.3 dB under ambient light conditions. Similarly, in the wearable experiment, the SNR is equally good for the LED strip at 9 and 12 V under ambient light conditions (21.9 dB) and higher in dark conditions (23.8 and 27.4 dB, respectively). The side-emitting fiber exhibited a broader range from 42.7 down to 19.3 dB under ambient light and 42.9 down to 20.2 dB in dark conditions.

Figure 10 illustrates the SNR plots for the LED strip (12 V) and the LED-coupled side-emitting fiber in ambient light conditions for the wearable experiment. The peaks in the plot of the LED strip correlate with the positions of the individual LEDs on the strip, whereas the gradual decrease in the LED-coupled side-emitting fiber plot of the same figure occurs mainly due to a fundamental property of side-emitting fiber: the power decrease along its length as a proportional amount of power has already been emitted from the fiber.

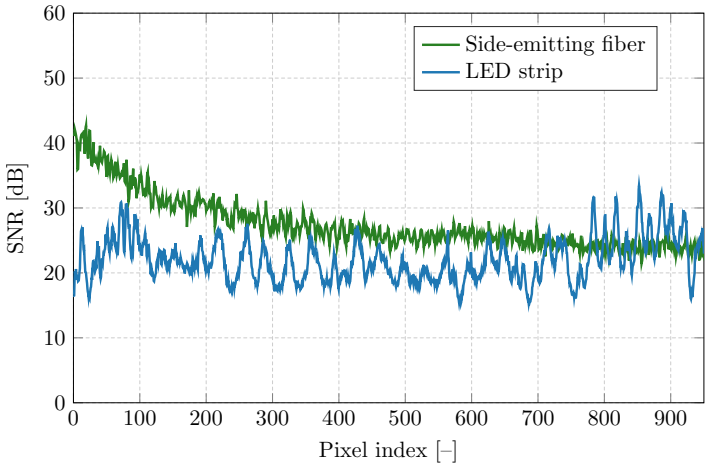

Fig. 10. Average signal-to-noise ratio (SNR) of the LED strip (12 V) and side-emitting fiber in ambient light conditions for the wearable experiment.

A general assumption about the communication link performance in OCC systems is that the bit error rate (BER) should be below 3.8×10^{-3}, the forward error correction (FEC) limit [35].

Optics EXPRESS

In the case of an OOK codification, assuming a Gaussian noise distribution environment, the relation of the BER and the SNR is expressed as BER = $Q(\sqrt{\text{SNR}})$ [36]. From this equation, the minimum SNR needed to ensure the required BER can be calculated; in this case, the SNR value is 12.2 dB. As can be seen from the experimental SNR results for all the measurement cases, the predicted system performance under optimal conditions is better than the FEC limit. Figure 11 shows the theoretical BER plot versus SNR, calculated from BER = $Q(\sqrt{\text{SNR}})$, considering the minimum measured SNR at 16 dB (from Fig. 10). The resulting BER for all cases is below 10^{-11}, which ensures high system performance in both LED strip and side-emitting fiber schemes.

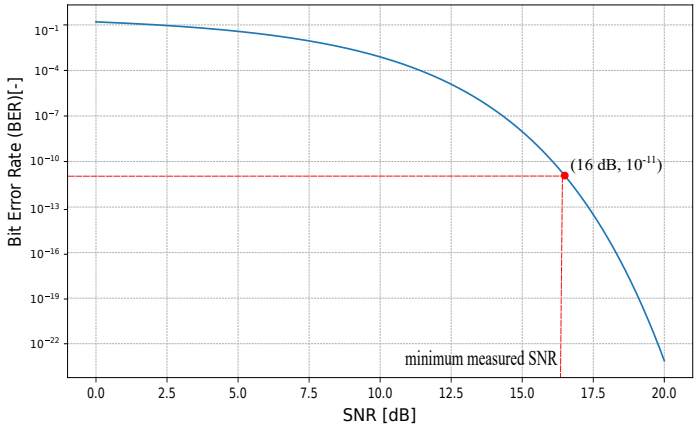

Fig. 11. Theoretical BER = $Q(\sqrt{\text{SNR}})$ with highlighted the minimum measured SNR 16dB.

Next, we analyzed the quality of the captured data in terms of the SoR, which is defined as the ratio of correctly decoded bits to the total number of transmitted bits [17]. Note, that the SoR is calculated from the correlation results in a dataset of 10 frames, equating to a total of 180 bits that we compare to the transmitted template. It is worth noting that the number of frames, in this case, was taken according to the experimental procedure, while in a real system, it would be a video recording of 30 frames per second, giving approximately 0.5 kbps. We considered that the detection of the template failed when we received less than 2 complete packets per frame. Consequently, the value of any dataset below 66.6 % is considered as 'no detection'.

The calculated SoR is depicted in Table 4 and Table 5 for the laboratory and wearable experimental setup, respectively. Note that the LED strip was measured under ambient light conditions in both experimental setups, while the LED-coupled side-emitting fiber measurements were conducted in darkness.

From the obtained values, we can conclude that the LED strip (12 V) generally results in higher SoR than the LED strip (9 V) and comparable SoR with the LED-coupled side-emitting fiber considering Method 2.

Regarding the laboratory experimental setup, the SoR of the LED strips is consistently high, close to 100 %. The LED-coupled side-emitting fiber using Method 1 exhibits variable and relatively lower SoR, spanning from approximately 72.2 % to 98.8 %. Once using the alternative image processing method (Method 2) produces improved results for the LED-coupled side-emitting fiber, rendering it comparable to the LED strip (12 V) outcomes.

Regarding the SoR values of the wearable experimental setup, we observe a decrease compared to the laboratory setup due to the reduced T_x length, which is caused by the limited amount of space on a T-shirt (100 cm transmitter length in laboratory setup vs. 50 cm in wearable setup). The LED strip (12 V) achieves SoR exceeding 88.8 %, while the LED strip (9 V) SoR exceeding 81.1 %. Based on Method 1, the LED-coupled side-emitting fiber demonstrates more SoR

Optics EXPRESS

Table 4. Success of reception (SoR) in the laboratory experimental setup.

x [m]	y [m]	Strip (9 V)	Strip (12 V)	Fiber (Method 1)	Fiber (Method 2)
0.0	2.5	<66.6 %	-	<66.6 %	78.3 %
0.4	2.4	89.8 %	-	86.6 %	96.7 %
0.8	2.3	96.2 %	-	75.8 %	97.5 %
1.2	2.1	98.3 %	-	90.0 %	99.1 %
1.0	0.0	100 %	100 %	98.8 %	100 %
	0.5	100 %	100 %	72.7 %	100 %
	1.0	100 %	100 %	79.4 %	100 %
	1.5	99.4 %	99.4 %	72.2 %	100 %
	2.0	93.8 %	93.3 %	72.8 %	96.9 %
2.0	0.0	100 %	100 %	95.5 %	100 %
	0.5	100 %	100 %	87.5 %	99.3 %
	1.0	100 %	100 %	80.5 %	99.4 %
	1.5	100 %	100 %	86.6 %	98.8 %
	2.0	90.5 %	94.4 %	90.0 %	97.7 %

Table 5. Success of reception (SoR) in the wearable experimental setup.

x [m]	y [m]	Strip (9 V)	Strip (12 V)	Fiber (Method 1)	Fiber (Method 2)
0.0	2.0	86.1 %	91.6 %	82.2 %	<66.6 %
0.3	1.9	90.0 %	97.7 %	90.0 %	90.0 %
0.6	1.8	81.6 %	96.6 %	92.2 %	98.3 %
1.2	1.5	91.6 %	98.8 %	88.2 %	87.7 %
1.0	0.0	100 %	100 %	85.0 %	100 %
	0.5	99.4 %	100 %	91.1 %	100 %
	1.0	100 %	100 %	80.5 %	100 %
	1.5	99.4 %	100 %	93.3 %	98.3 %
	1.7	99.0 %	98.3 %	92.2 %	98.8 %
	2.0	89.4 %	92.7 %	94.1 %	98.3 %
2.0	0.0	95.5 %	95.0 %	78.8 %	100 %
	0.5	87.7 %	91.6 %	91.6 %	100 %
	1.0	81.1 %	88.8 %	90.0 %	100 %
	1.5	99.1 %	99.1 %	87.5 %	100 %
	2.0	94.1 %	93.3 %	89.8 %	93.5 %

fluctuations than the LED strip (12 V), ranging from approximately 78.8 % to 94.1 %. Conversely, with Method 2, the side-emitting fiber exhibits even superior performance compared to the LED strips. This result underscores the requirement of using Method 2 for side-emitting fibers in wearable OCC scenarios as they fundamentally differ in transmitter shape (not being a perfect line source and having illumination decay along the fiber length).

We noticed that the detection of the template failed at (0.0, 2.5) capturing position in the laboratory experimental setup (with Method 1), but not in the wearable, and this can be attributed to the visibility of the T_x's side. As mentioned earlier, in each setup (laboratory vs. wearable) a different position between the T_x and camera was tested. In general, in both experimental setups,

Optics EXPRESS

the best SoR is achieved at (1.0, 0.0) capturing position, when the camera and the T_x are aligned and in close distance.

5. Conclusion

In this paper, we experimentally evaluate two types of LED-based distributed transmitters, the LED strip and the LED-coupled side-emitting optical fiber, in both laboratory and wearable OCC systems. Evaluation encompasses power consumption (432 mW and 720 mW for the LED strip, and 525 mW for the side-emitting optical fiber), the success of reception, and the signal-to-noise ratio. The primary contribution of this research lies in the demonstration of two different technologies for wearable OCC both allowing for accurately detecting transmitted bits and showing critical aspects for the LED strip and side-emitting fiber placement and camera receiver position.

In conclusion, we identify some practical considerations that impact the performance of our system. Initially, the reduced power of illumination stems from the side-emitting fiber operating at a lower voltage. Furthermore, the side-emitting fiber's diameter of 4 mm is significantly smaller than the 1 cm diameter of the LED strip, resulting in a reduced illuminating area. On the other hand, the smaller diameter of the side-emitting fiber is more flexible, tolerating more movement in wearable applications. An additional aspect impacting practicality is the fact that the LED strip is more distributed electrically, whereas the side-emitting fiber only requires circuitry at one end, allowing for a more compact design.

The proposed setup was tested using standard devices, which makes it applicable for widespread use. Our future research will encompass the implementation of a wearable device seamlessly integrated into clothing and combined with sensors to transmit real health data. Additionally, we plan to integrate wavelength division multiplexing techniques, where the template can act as a beacon for transmitting data across multiple light wavelengths. Furthermore, we will experiment a wearable setting with user in motion. Lastly, employing the latest smartphone versions capable of capturing video with reduced exposure time and higher frame rates. The global shutter capturing mechanism of smartphones enables simultaneous video streaming and data acquisition, which could enable lower power consumption transmitters to operate over longer distances.

Funding. Agencia Canaria de Investigación, Innovación y Sociedad de la Información (APCR2022010014); NEWFOCUS COST action (CA19111); České Vysoké Učení Technické v Praze (SGS23/168/OHK3/3T/13); Agencia Estatal de Investigación (TED2021-130049B-C21, PID2020-114561RB-100).

Acknowledgment. The authors also thank for his technical support, Mr. Daniel Dousek from Czech Technical University.

Disclosures. The authors declare no conflicts of interest.

Data availability. Data underlying the results presented in this paper are not publicly available at this time but may be obtained from the authors upon reasonable request.

References

1. "IEEE standards association," https://standards.ieee.org/ieee/802.15.7a/10367/. Accessed: 2023-09-15.
2. M. Z. Chowdhury, M. T. Hossan, M. Shahjalal, *et al.*, "A new 5G ehealth architecture based on optical camera communication: An overview, prospects, and applications," IEEE Consumer Electron. Mag. **9**(6), 23–33 (2020).
3. N.-T. Le and Y. M. Jang, "Performance evaluation of MIMO optical camera communications based rolling shutter image sensor," in *2016 Eighth International Conference on Ubiquitous and Future Networks (ICUFN)*, (2016), pp. 140–144.
4. "Statcounter," https://gs.statcounter.com/screen-resolution-stats/mobile/worldwide. Accessed: 2023-09-15.
5. R.-A. Dobre, R.-O. Preda, and R.-A. Badea, "Robust occ system optimized for low-frame-rate receivers," Sensors **22**(16), 5938 (2022).
6. Y. Wang, S. Cang, and H. Yu, "A survey on wearable sensor modality centred human activity recognition in health care," Expert Syst. with Appl. **137**, 167–190 (2019).
7. S. Majumder, T. Mondal, and M. J. Deen, "Wearable sensors for remote health monitoring," Sensors **17**(12), 130 (2017).

Optics EXPRESS

8. J. S. Heo, M. F. Hossain, and I. Kim, "Challenges in design and fabrication of flexible/stretchable carbon-and textile-based wearable sensors for health monitoring: A critical review," Sensors **20**(14), 3927 (2020).
9. S. Nasiri and M. R. Khosravani, "Progress and challenges in fabrication of wearable sensors for health monitoring," Sensors Actuators A: Phys. **312**, 112105 (2020).
10. R. De Fazio, M. De Vittorio, and P. Visconti, "Innovative IoT solutions and wearable sensing systems for monitoring human biophysical parameters: a review," Electronics **10**(14), 1660 (2021).
11. S. Kharche and J. Kharche, "6G intelligent healthcare framework: A review on role of technologies, challenges and future directions," Journal of Mobile Multimedia **19**, 603–644 (2023).
12. T. Adiono, R. F. Armansyah, S. S. Nolika, *et al.*, "Visible light communication system for wearable patient monitoring device," in *2016 IEEE Region 10 Conference (TENCON)*, (2016), pp. 1969–1972.
13. C. Le Bas, T. B. Hoang, S. Sahuguede, *et al.*, "Lighting fixture communicating in infrared and visible for indoor health monitoring," in *2017 IEEE 19th International Conference on e-Health Networking, Applications and Services (Healthcom)*, (2017), pp. 1–6.
14. T. B. Hoang, S. Sahuguede, and A. Julien-Vergonjanne, "Optical wireless network design for off-body-sensor based monitoring," Wirel. Commun. Mob. Comput. **2019**, 1–13 (2019).
15. M. J. Hasan, M. A. Khalighi, J. García-Márquez, *et al.*, "Performance analysis of Optical-CDMA for uplink transmission in medical extra-WBANs," IEEE Access **8**, 171672–171685 (2020).
16. S. Chen, J. Qi, S. Fan, *et al.*, "Flexible wearable sensors for cardiovascular health monitoring," Adv. Healthcare Mater. **10**(17), 2100116 (2021).
17. S. R. Teli, K. Eollosova, S. Zvanovec, *et al.*, "Optical camera communications link using an LED-coupled illuminating optical fiber," Opt. Lett. **46**(11), 2622–2625 (2021).
18. K. Eöllos-Jarošíková, V. Neuman, C. M. Jurado-Verdú, *et al.*, "Long-distance indoor optical camera communication using side-emitting fibers as distributed transmitters," Opt. Express **31**(16), 26980 (2023).
19. A. Reupert, J. Schröder, and L. Wondraczek, "Radiation from side-emitting optical fibers and fiber fabrics: Radiometric model and experimental validation," Adv. Photonics Res. **3**(4), 2100104 (2022).
20. S. L. Logunov, K. W. Bennett, E. J. Fewkes, *et al.*, "Silica nano-structured fiber for illumination," J. Lightwave Technol. **37**(22), 5667–5673 (2019).
21. M. Lanzarini-Lopes, S. Garcia-Segura, K. Hristovski, *et al.*, "Particle-modified polymeric cladding on glass optical fibers enhances radial light scattering," J. Opt. Soc. Am. B **36**(6), 1623 (2019).
22. W. S. Klubben, S. L. Logunov, E. J. Fewkes, *et al.*, "Novel light diffusing fiber for use in medical applications," in *SPIE Proceedings*, I. Gannot, ed. (SPIE, 2016).
23. B. Selm, E. A. Gürel, M. Rothmaier, *et al.*, "Polymeric optical fiber fabrics for illumination and sensorial applications in textiles," J. Intell. Mater. Syst. Struct. **21**(11), 1061–1071 (2010).
24. V. Georlette, F. Piras, C. Jurado-Verdu, *et al.*, "Content triggering system using tricolor led strips and optical camera communication in rolling shutter mode," in *2021 Third South American Colloquium on Visible Light Communications (SACVLC)*, (2021), pp. 01–06.
25. F. Cocconcelli, G. Matrella, N. Mora, *et al.*, "IoT smart flooring supporting active and healthy lifestyles," Sensors **23**(6), 3162 (2023).
26. M. Domonkos, Z. Dombi, and J. Botzheim, "Led strip based robot movement intention signs for human-robot interactions," in *2020 IEEE 20th International Symposium on Computational Intelligence and Informatics (CINTI)*, (IEEE, 2020), pp. 121–126.
27. J. He, K. Yu, Z. Huang, *et al.*, "Multi-column matrices selection combined with k-means scheme for mobile occ system with multi-leds," IEEE Photonics Technol. Lett. **33**(12), 623–626 (2021).
28. V. Matus, V. Guerra, C. Jurado-Verdu, *et al.*, "Wireless sensor networks using sub-pixel optical camera communications: Advances in experimental channel evaluation," Sensors **21**(8), 2739 (2021).
29. V. Matus, V. Guerra, C. Jurado-Verdu, *et al.*, "Demonstration of a sub-pixel outdoor optical camera communication link," IEEE Latin Am. Trans. **19**(10), 1798–1805 (2021).
30. Atmel, "XIAO SAMD21, 32-bit 48MHz microcontroller (SAMD21G18) with 256KB flash, 32KB SRAM," Datasheet (2016).
31. A. Nano, "ATmega328 16 MHz, 2KB SRAM, 32KB flash, 1KB EEPROM," Datasheet (2023).
32. Samsung, "Samsung galaxy A51 Dual SIM (4GB/128GB)," https://www.samsung.com/gr/smartphones/galaxy-a/galaxy-a51-blue-128gb-sm-a515fzbveue/ (2021). Accessed: [2023-10-02].
33. T. Le, N.-T. Le, and Y. M. Jang, "Performance of rolling shutter and global shutter camera in optical camera communications," in *2015 International Conference on Information and Communication Technology Convergence (ICTC)*, (IEEE, 2015), pp. 124–128.
34. C. Jurado-Verdu, V. Matus, J. Rabadan, *et al.*, "Correlation-based receiver for optical camera communications," Opt. Express **27**(14), 19150–19155 (2019).
35. P. Luo, M. Zhang, Z. Ghassemlooy, *et al.*, "Undersampled-based modulation schemes for optical camera communications," IEEE Commun. Mag. **56**(2), 204–212 (2018).
36. M. Gismalla, M. Abdullah, W. A. Mabrouk, *et al.*, "Data rate and ber analysis for optical attocells configuration model in visible light communication," in *2019 International Conference on Information Science and Communication Technology (ICISCT)*, (2019), pp. 1–6.